Final Draft
of the original manuscript:

Witte, F., Feyerabend, F.; Maier, P.; Fischer, J.; Stoermer, M.; Blawert, C.; Dietzel, W.; Hort, N.:

Biodegradable magnesium–hydroxyapatite metal matrix composites

In: Biomaterials (2007) Elsevier

DOI: 10.1016/j.biomaterials.2006.12.027

Magnesium-hydroxyapatite Composites:

A Novel Approach to Biodegradable Metals.

F.Witte, F.Feyerabend, J.Fischer, P.Maier, M.Stoermer, C.Blawert, W.Dietzel, N.Hort

Abstract

Recent studies indicate that there is a high demand to design magnesium alloys with adjustable corrosion rates and suitable mechanical properties. A novel approach to this challenge might be the application of metal matrix composite (MMC) based on magnesium alloys. In this study, a MMC made of magnesium alloy AZ91D as a matrix and hydroxyapatite (HA) particles as reinforcements have been investigated in vitro for mechanical, corrosive and cytocompatible properties. The mechanical properties of the MMC-HA were adjustable by the choice of HA particle size and distribution. Corrosion tests revealed that HA particles stabilized the corrosion rate and exhibited more uniform corrosion attack in artificial sea water and cell solutions. The phase identification showed that all samples contained hcp-Mg, $Mg_{17}Al_{12}$, and HA before and after immersion. After immersion in artificial sea water $CaCO_3$ was found on MMC-HA surfaces, while no formation of $CaCO_3$ was found after immersion in cell solutions with and without proteins. Co-cultivation of MMC-HA with human bone derived cells (HBDC), cells of an osteoblasts lineage (MG-63) and cells of a macrophage lineage (RAW264.7) revealed that RAW264.7, MG-63 and HBDC adhere, proliferate and survive on the corroding surfaces of MMC-HA. In summary, MMC-HA are novel cytocompatible biomaterials with adjustable mechanical and corrosive properties.

Keywords

magnesium, hydroxyapatite, metal matrix composite, corrosion, mechanical properties, cytotoxicity

1. Introduction

Previous in vivo studies have shown that magnesium alloys are a suitable new class of biodegradable metal implants. Current research indicates that there is a high demand to design magnesium alloys with adjustable in vivo corrosion rates while the mechanical properties are not compromised or even enhanced. A novel approach to this challenge might be the application of metal matrix composite (MMC) based on magnesium alloys. The MMCs have gained increasing interest in the last decade particularly in automotive applications and general transportation based on their higher specific stiffness, strength, creep resistance and minimized sensibility to galvanic corrosion [1]. The advantage to use MMCs as biomaterials are the adjustable mechanical properties (young`s modulus, tensile strength) as well as the adjustable corrosion properties by choosing the appropriate composites [2;3]. An appropriate way to control magnesium corrosion is to elevate the surrounding pH of the magnesium alloy to stabilize the corrosion products in the protective corrosion layer. Especially calcium is known to reduce the susceptibility of magnesium to corrode when added in amounts of a few tenths of weight percents [4;5]. As a natural bone composition, hydroxyapatite (HA) is known to possess a low solubility in body environment [6;7]. Therefore, HA particles seem to be suitable as reinforcements in magnesium based MMCs. In previous studies the magnesium alloy AZ91D has revealed local corrosion attack in vitro and in vivo [8;9]. In this study a metal matrix composite made of AZ91D as a matrix and HA particles as reinforcements have been investigated in vitro for mechanical and corrosive properties. The cytocompatibility of this novel MMC-HA in MTT assays [10] has been investigated by cocultivation of material samples with human bone derived cells (HBDC), an osteoblast lineage (MG-63) and a macrophage lineage (RAW264.7).

2. Materials and Methods

2.1. Material production

The MMCs were produced by mixing 20 wt% of hydroxyapatite powder (particle size < 44 µm, Alfa Aesar GmbH, Germany) and the balance of powdered magnesium alloy AZ91D into an AZ31 can of 70 mm diameter. The initial particle size of magnesium alloy AZ91D was approximately 30 µm. Subsequently, this packet was extruded at 400°C to a diameter of 18 mm. Material samples were machined from the extruded rod.

2.2. Mechanical and metallurgical testing

Vickers hardness measurements ($HV_{0.1}$) and nanoindentation (load of 1000 µN) have been carried out for mechanical characterization of the material. Vickers hardness measurements ($HV_{0.1}$) have been done with a standard microhardness tester (Microhardness tester, Carl Zeiss, Germany). Nanoindentation, using a modified scanning force microscope as a triboscope (Hysitron Triboscope^{TM}, Hysitron Incorporated, USA), has been employed and this technique allows very small regions to be investigated and different phase structures to be distinguished. Furthermore, the Young's modulus can be determined by nanoindentation. Microstructural investigation has been done by various analysis methods. Optical microscopy has been performed to get an overview of distribution and size of components within the material. Scanning electron microscopy (JEOL JSM-6400 SEM, JEOL Ltd, Japan), in detail EDX analyses, has been carried out to evaluate the composition of defined areas in the microstructure. The sample preparation is reported briefly: Cross and longitudinal sections were ground with water and ethanol down to a graining size of 1200, polished with a lubricant containing 3 µm diamond particles followed by a lubricant containing 1 µm diamond particles under addition of dish liquid (Struers GmbH, Willich, Germany). They were etched first with 10 % nital for a few seconds to clean off remains in the ultrasound bath and then etched with a solution from ethanol, distilled water and picric acid [11].

2.3. Corrosion testing

Specimen preparation for corrosion tests

The cylindrical specimens of 10 mm diameter and 5 mm thickness were machined from the extruded rods. The two flat cylinder surfaces were grinded with 1200 grid SiC paper and cleaned in ethanol prior to corrosion tests. For the immersion tests a 1 mm diameter hole was drilled into the specimens providing a fixture for the specimens during testing.

Immersion Testing

Immersion testing was performed for 24 and 72 hours in artificial sea water (28g NaCl, 5g $MgCl_2 \cdot 6H_2O$, 2.4g $CaCl_2 \cdot 6H_2O$, 7g $MgSO_4 \cdot 7H_2O$ and 0.2g $NaHCO_3$ in 985 ml distilled water, DIN 50905), Dulbecco`s modified eagle medium (DMEM, Invitrogen Corporation, Germany) herein called cell solution and cell solution with proteins (10% fetal bovine serum, FBS, PAA Laboratories, Linz, Austria) at 37°C. Three specimens for each condition were immersed in 200 ml of solution, without touching the container wall or each other. The solution temperature was controlled by a flow of heated water in a water bath in which the container were placed (37 ± 0.2°C). The electrolyte was not stirred during the experiments and saturated with atmospheric oxygen. The corrosion rates were determined by weight loss measurements using chromic acid for removing the corrosion products.

Electrochemical testing

The electrochemical tests were performed in artificial sea water at 37°C on flat cylindrical surfaces (perpendicular to the extrusion direction) using an ACM Gill AC potentiostat (ACM Instruments, Cumbria, UK). A sequence of tests, starting with 30 min measurement of the rest potential, followed by a single potentiodynamic polarisation and 72 single electrochemical impedance spectroscopy measurements (EIS) was used with 1 hour rest between each measurement. The electrolyte temperature was controlled by a flow of heated water in the double wall (37 ± 0.2°C) of the electrolytic cell with an electrolyte volume of 333 ml. The electrolyte was stirred during the experiments and saturated with atmospheric oxygen. A three electrode set-up with an Ag/AgCl reference and a platinum counter electrode

was used. After 30 min recording of the free corrosion potential, the polarization scan was started from -200 mV relative to the free corrosion potential with a scan rate of 0.2 mV/s. The test was terminated when a corrosion current density of 0.1 mA/cm^2 was exceeded. From the cathodic branch of the polarization curve the corrosion rate was determined using the Tafel slope. The low terminating limit was chosen to minimize the corrosion attack on the surface before the long term EIS measurements have been started. The EIS measurements were carried out over a frequency range from 30 kHz to 0.1 Hz. The amplitude of the sinusoidal signals was 10 mV. The resistance values (charge transfer resistance) obtained at 0° phase shift were used as an indicator of the corrosion resistance of the specimens.

2.4. XRD analysis

The samples were investigated by means of X-ray diffraction (XRD) in parallel beam geometry, using Cu-$K_{\alpha 1}$ radiation (wavelength λ=1.5406Å). The X-ray diffractometer (D8 Advance from Bruker AXS, Karlsruhe) with a line focus was equipped with a Göbel mirror and a 1 mm slit on the primary side. Because of the reflectometry stage of the diffractometer, the samples were aligned exactly at the goniometer center. On the secondary side, there are a 0.6 mm backscattering slit and a 0.2 mm detector slit. The diffraction patterns were measured from 2 Θ (8 - 92°) for each sample. The increment was 0.04° and the step time was 16s. The determination of the lattice parameter has shown a precision of better than 0.01 Å. For the qualitative phase identification, the database PDF-2 (Release 2002) from the International Center for Diffraction (ICDD) was used [12].

2.5. Synchrotron-radition based microtomography (SRμCT)

For SRμCT the experimental set-up at the Hamburger Synchrotronstrahlungslabor (HASYLAB) at Deutsches Elektronensynchrotron (DESY) was used at beamline BW2 at a photon energy of 24 keV. To perform in-situ corrosion measurements a cuvette was made of a radiation resistant plastic (PEEK) to contain the corrosive solution and the magnesium sample during the tomographic measurements. Artificial sea water with an initial pH of 7.4 and a

temperature of 37°C was used as a corrosive solution. The corrosive solution in the cuvette was constantly exchanged (50ml/min) by a peristaltic pump from a reservoir with constant temperature and pH. Cylindrical sample were machined from MMC-HA (3.02 mm diameter, 5.0 mm height) and AZ91D (3.13 mm diameter, 5.0 mm height) for in-situ corrosion measurements. Both samples were immersed in a cuvette and attenuation images were acquired every 45 minutes during a period of 20 hours. The initial sample volumes used to observe the corrosion were slightly different due to limited machining abilities (MMC-HA: 12.93 mm^3; AZ91D: 13.81 mm^3). The data transfer from the CCD was accelerated by double binning of the image data. Furthermore, a step-size of 0.5° rotation angle was chosen to decrease the overall time for scanning a single tomogram to 30 minutes for a rotational range from 0° to 180°. A voxel edge length of 4.7 µm was obtained. Changes in surface morphology, remaining metallic sample volume were observed and the corrosion rate was calculated according to equation 1 [9]:

$$CR = \frac{\Delta V}{A \cdot t} \qquad \text{(Eq.1)}$$

, where CR is the corrosion rate, ΔV is the loss of the metal volume during the corrosion test, A the initial surface area, and t is the immersion time.

2.6. Cytocompatibility tests

The change in pH of the cell culture medium with immersed MMC-HA samples, tissue culture plastic or without any samples was measured using a calibrated IQ 150 pH-meter (IQ Scientific Instruments, San Diego, USA). The measurements were performed in 10 replicates from different vials parallel to cell culture experiments.

2.6.1. Isolation and culture of cells

Human bone derived cells (HBDC)

HBDC were grown out of bone chips obtained from patients undergoing total hip arthroplasty according to the protocol of Gallagher [13]. The isolation was performed in accordance to the

local ethic committee. In brief, cancellous bone was cut into chips of about 5 mm, and cultured in Dulbecco's modified eagle medium (DMEM) and Glutamax-I (Invitrogen Corporation, Germany) with 10 % fetal bovine serum (FBS; PAA Laboratories, Linz, Austria), 1 % penicillin and 100 µg/ml streptomycin (Invitrogen Corporation, Germany) for about 10 days without changing the cell culture medium. When HBDCs started to grow out of the bone chips, medium was changed every three days. Passaging was done at 70-80 % confluence. Experiments were performed with cells of the first passage.

MG-63 cells

The human osteosarcoma cell line MG-63 was cultured in the same cell culture medium as HBDC. Cells were passaged at subconfluency (70-80%) and reseeded in a density of $2 \cdot 10^4$ cells/cm^2. For the experiments cells of the 5th passage were used.

RAW 264.7 cells

The mouse tumor-derived macrophage cell line was cultured in DMEM containing low glucose with 10% FBS. Passaging was done when the cells reached a confluence of about 60-70%. They were reseeded in a density of $1 \cdot 10^4$ cells/cm^2. Cells of the 6th passage were used for the experiments.

2.6.2. Sample Sterilization

The samples were sterilized by gamma-irradiation at the nuclear facility of the GKSS Research Center Geesthacht with a total dosage of 29 kGy.

2.6.3. Direct and preincubation cell assay

Direct assay

The material samples were handled in a sterile environment. Prior to cell seeding the carriers were transferred to 12-well plates, which were coated with agarose to minimize unspecific cell adhesion. In the control groups the wells were not coated, so the control value is that of tissue culture plastic. Then, $5 \cdot 10^4$ cells (MG-63, RAW 264.7) or $2 \cdot 10^4$ cells (HBDC) were

seeded onto the magnesium samples and were allowed to settle for 30 minutes for initial cell adhesion. After seeding the magnesium samples with cells, the samples were covered with 3 ml medium and incubated at 37°C and 5% CO_2 for 2 days (MG-63, RAW 264.7) and 3 days (HDBC), respectively. At the end of the experiments an MTT assay was performed to measure cell viability.

Preincubation assay

The preincubation assay differed from the direct assay in that the magnesium samples were incubated for two days in cell culture medium prior to cell seeding. Afterwards, the same procedure as in the direct assays was applied.

2.6.4. MTT-assay

The measurement of metabolic cell activity was used to compare the cell viability after initial cell adhesion and proliferation on preincubated and not-preincubated magnesium samples as well as and on tissue culture plastic. Metabolic activity was determined by the cell proliferation kit MTT (Roche Diagnostics GmbH, Mannheim, Germany). The MTT-assay is based on the cleavage of the yellow tetrazolium salt MTT (thiazolyl blue tetrazolium bromide) into purple formazan by metabolically active cells. In brief, the different samples were incubated for two (MG-63, RAW 264.7) or three (HDBC) days in 3 ml DMEM in 12-well plates. Then, a medium change was performed and 1.5 ml fresh medium was supplemented to the wells. Afterwards, 150 µl of the MTT-solution (5 mg/ml in phosphate buffered saline, PBS) was added. After an incubation period of 4 hours the cells were lysed and the formazan crystals solubilized by adding 1.5 ml solubilization solution (10% SDS in 0.01M HCl). This was followed by an incubation overnight in a humidified atmosphere (37°C, 5% CO_2). The solubilized formazan product was quantified photometrically quantified using an ELISA reader (Tecan Sunrise, TECAN Deutschland GmbH, Crailsheim, Germany) at 570 nm with a reference wavelength of 655 nm.

2.6.5. Statistics

Statistical differences between groups were determined using ANOVA. Statistical significance was defined as $p < 0.05$.

3. Results

3.1. Mechanical and metallurgical characterization

The microstructure of the MMC-HA sample in longitudinal direction revealed that the grains appeared as horizontal elongated grains in the extrusion direction (Fig. 1). The magnesium matrix microstructure consisted of small grains of a size of a few micrometers (1-5µm). Furthermore, bands of larger grains were observed, where shear forces during processing have not been fully applied and an incomplete deformation of initial powder particles remained (Fig. 2a). Apatite conglomerations were inhomogenously spread over the sample, seen as black formations of various sizes (Fig. 1, 2). The size differed from less than a micrometer up to 20 µm and even more if agglomerated. However, a few apatite formations showed possible facets of crystallized areas.

The apatite formations appeared to be very brittle and were difficult to indent without damaging them. The Vickers hardness indentations had a size of approximately 30 µm. The average $HV_{0.1}$ of the apatite conglomerates was 111, while the average $HV_{0.1}$ of the MMC-HA was 73. However, single hardness values varied from 63 to 98 depending on the contribution and size of apatite conglomerates. Low hardness ($HV_{0.1}$ 63) was observed with large and inhomogenously distributed conglomerates (Fig. 2a), while finer and more homogenously distributed conglomerates (Fig. 2b) lead to higher hardness ($HV_{0.1}$ 98). This shows that size and distribution of the HA particles can change the overall hardness of the composite material compared to standard magnesium alloys (up to $HV_{0.1}$ 80). The Young's modulus of the MMC-HA matrix has been measured with nanoindentation at 40 GPa, which is typical for magnesium alloy AZ91D.

The EDX analysis of a representative area of the matrix revealed a typical composition for an AZ91D magnesium alloy, except the slightly enriched calcium, which could be attributed to the apatite additions (Fig. 3a). A representative EDX analysis of an apatite conglomerate revealed amounts of phosphorous and calcium which are typical for calcium phosphate or

rather hydroxyapatite (Fig. 3b). The representative areas of magnesium matrix and apatite formation were clearly identified by EDX analysis (Table 1).

3.2. Corrosion testing

Immersion Testing

The weight change of the specimens was measured after 24 and 72 hours of immersion in artificial sea water and cell solutions with and without protein addition (Fig. 4). The specimens in artificial sea water exhibited severe corrosion attack (Fig. 4) which is consistent with a large weight gain and a rough surface covered with various corrosion products. In contrast, the specimens immersed in cell solutions with and without protein revealed glassy surface layers with black underlayers which were formed on the specimens. Small weight changes could be measured in these samples. The protein addition to the cell solution resulted in a visible gas evolution at the beginning of the immersion test, which stopped after a couple of hours. After the removal of the corrosion products with chromic acid the weight loss indicated that there was corrosion attack on all specimens (Fig. 4). The maximum weight loss was observed for the specimens immersed in sea water, followed by immersion in cell solution with protein addition and by pure cell solution. The specimens in artificial sea water (Fig. 5 a,c) suffered from strong localised corrosion attack, while all the specimens in cell solution showed a more uniform corrosion attack (Fig. 5 b,d). The conversion of the weight losses into corrosion rates revealed that in all solutions the corrosion rate is decreasing with increasing immersion time (Fig. 6).

Electrochemical Testing

The short term polarisation measurements resulted in a corrosion rate of 1.25 ± 0.16 mm/year which were lower than the corrosion rates (2.0-3.2 mm/yr) determined in the immersion test. The long-term behaviour was studied over 72 hours with EIS measurements performed every hour. There was a general trend that the charge transfer resistance was increasing from about

1000 Ωcm^2 to 1300 Ωcm^2 with longer immersion times. However, a larger scatter was found ranging from 750 to 1600 Ωcm^2 (Fig. 7) occurring randomly over the whole test period.

3.3. XRD analysis

To characterize the raw material, pure hydroxyapatite powder was investigated first. The diffraction pattern (Fig. 8a) showed the reflections expected for hydroxyapatite $Ca_{10}(PO_4)_6(OH)_2$ (Fig. 8a, see 74-565). The unit cell of the listed hydroxyapatite phase was hexagonal and the lattice parameters were a=9.424Å and c=6.879Å [14]. The strong lines of hydroxyapatite were in the range of 2 Θ = 25° to 55°. Because of the long a-axis of the unit cell, we have been able to measure a diffraction peak at 10.8° from the (1.00)-planes. The diffraction pattern of the extruded MMC-HA (Fig. 8b) exhibited dominant hcp-Mg reflections. In addition, there were reflections from the $Mg_{17}Al_{12}$-phase (Fig. 8a), which originated from the AZ91D matrix and clear reflections from hydroxyapatite could be observed (Fig. 8a). Thus, hydroxyapatite could still be detected in the extruded MMC. Weak indications of other phases have been found, which correspond with the positions expected for calcium hydrogen phosphates or calcium phosphates.

After immersion testing in artificial sea water for 24 and 72 hours, diffraction patterns were performed (Fig. 9a). There were again reflections from hcp-Mg, $Mg_{17}Al_{12}$, hydroxyapatite, $CaCO_3$ and $Mg(OH)_2$, which were used to determine the structures of the first three phases. The following lattice parameters were determined: a=3.19Å and c=5.20Å for hcp-Mg and a=10.59Å for bcc-$Mg_{17}Al_{12}$. The diffraction pattern of hydroxyapatite matches again quite well to the pattern 74-565 from the PDF-2 database: a=9.424Å and c=6.879Å. The positions of the reflections from the hydroxyapatite particles have been found to match nearly those of the powdered sample (Fig. 8a). However, some new reflections at 2θ=26.1°, 27.1°, 33.0° and 45.8°, belonging to a new orthorhombic phase were found (Fig. 9a). The lattice parameters were determined at a=4.97Å, b=8.00Å and c=5.76Å. Based on the components of the artificial sea water, calcium carbonate was identified by means of phase determination. After

immersion testing for 24 and 72 hours in cell solutions without and with protein (Fig. 9 b,c), the diffraction patterns were quite similar to that of the non-immersed MMC-HA sample (Fig. 8b). The reflections can again clearly be assigned to hcp-Mg, bcc-$Mg_{17}Al_{12}$, and hydroxyapatite. No reflections from $CaCO_3$ were found after immersion in cell solution with and without protein addition. At lower 2Θ angles, the background was increased and the peaks were broadened which might be due to the fact that the respective top layers were amorphous (Inserts in Fig. 9 b,c).

3.4. Synchrotron-radiation based tomography

In general, minor corrosion attack occurred on the MMC-HA compared to the AZ91D matrix sample (Fig. 10). Initial pit formation was observed 2-3 hours after immersion in artificial sea water. The small pits continuously grew until 9 hours after immersion, while high X-ray absorbent precipitaitions were observed to accumulate on the MMC-HA surface until the end of the experiment. EDX and XRD analysis revealed that these precipitations consisted of calcium carbonate. The surface of the MMC-HA was almost fully covered by $CaCO_3$ after 9 hours and the growth rate of the pits decreased nearly completely (Fig. 11). The AZ91D sample exhibited severe pitting after immersion in artificial sea water. The pits grew faster and deeper than in the MMC-HA sample (Fig. 10). The precipitations were found on uncorroded surfaces as well as a cover on some shallow pits. The observed sample volume of AZ91D decreased about 2.31% (0.32 mm^3) of its metal volume after 20 hours of immersion, while the change in the observed sample volume of the MMC-HA was too low for a reliable determination. Artifacts from small high absorbing areas occurred during the reconstruction procedure and interfered with the thin corrosion layer of the MMC-HA sample. Therefore, the number of voxels changing their grey values according to the corrosion products was too low to calculate a reliable change in the MMC-HA sample volume (Fig. 11). In contrast, the prominent corrosion of AZ91D in artificial sea water facilitated the calculation of the corrosion rate (7.94 mm/yr) according to equation 1 [9].

3.5. Cytocompatibiliy tests

The MMC-HA samples were either directly seeded with cells or cell seeding was performed after 2 days of preincubation in cell culture media. During this time, the MMC-HA samples were covered by a dense black corrosion layer with some crystalline depositions and no gas evolution was observed further on. The influence of the corrosion on medium buffer capacity was determined by the pH-value after 2 days of preincubation. It could be demonstrated, that pH values were higher for medium incubated with tissue culture plastic and MMC-HA than for the fresh control medium without any samples (Table 2).

The results obtained for cell viability in MTT tests were different for human bone derived cells (HBDC), osteoblasts (MG-63) and macrophages (RAW 264.7). The viability of RAW 264.7 was in the range of the control in the direct assay, but higher MTT values were obtained from the preincubation assay (Fig. 12). The direct seeding of MG-63 on MMC-HA led to higher MTT values (ANOVA, $n = 16$, $p < 0.05$) than for MG-63 seeded on tissue culture plastic. In contrast, a preincubation of MMC-HA led to lower increase of MTT value for MG-63 than in the direct assay.

HBDC showed no differences between the direct and preincubation assay (ANOVA, $n = 9$, $p > 0.05$), however the viability of HBDC directly seeded on MMC-HA as well as on preincubated MMC-HA exceeded the viability of HBDC seeded on tissue culture plastic.

4. Discussion

In this study we have demonstrated that magnesium alloy-based metal matrix composites (MMC) using the magnesium alloy AZ91D as a matrix and hydroxyapatite (HA) as reinforcements demonstrated appropriate mechanical, corrosive and cytocompatible properties. Since the control of in vivo corrosion is of major importance, the use of MMC-HAs provide a wide range of biodegradable magnesium alloys possessing adjustable properties for future load bearing applications in musculoskeletal surgery.

The matrix microstructure of the investigated MMC-HA consisted of small grains of a size of a few micrometers which is typical for extruded magnesium alloys with an initial particle size of 10 - 30 µm. The microstructural analyses showed an inhomogeneous distribution of HA particles within the AZ91D magnesium matrix, which resulted in locally different hardness and thus in locally different mechanical properties. A more homogenous distribution of HA particles is favourable, which will result in a more homogenous corrosion process as well as in more homogenously distributed mechanical properties. Measurements of micro- and nano-hardness (Vickers Hardness) have been shown in previous studies to have a strong positive relationship with Young's modulus, yield stress and ultimate stress [15;16]. The measurements showed that HA particle distribution influenced the overall hardness of the composite material compared to standard magnesium alloys in general. A limitation of the nano-indentation measurement in this study was that the diamond tip could slip off the HA formation, or even shifting them, resulting in wrong hardness values. The Vickers hardness for magnesium alloys is reported to have $HV_{0.1}$ values up to 80 [17;18] and was measured in this study to have an average $HV_{0.1}$ value of 73. Due to the brittleness and lose contact of the HA conglomerates in the MMC-HA matrix, the tensile and compressive strength of the composite is not expected to be significantly higher than of non-reinforced magnesium alloys. Since the microhardness of cortical bone is reported be about 49.8 [19], the tested MMC-HA seemed to be in closer agreement to the characteristics of the natural bone, which compressive

yield strength is 130-180 MPa [20]. Especially large load bearing implants will profit from the locally adjustable properties of MMC-HA.

In contrast to other magnesium alloy-based metal matrix composites, the corrosion rate of the magnesium matrix AZ91D was not enhanced by HA particles [21;22]. Only rare localized corrosion attack have been observed by SRμCT on the MMC-HA sample during the first 20 hours of immersion in artificial sea water, while a comparable AZ91D matrix sample exhibited severe localized corrosion. The corrosion rates of MMC-HA was found to differ depending on the measurement system used and should be mentioned in further studies. The short term polarisation measurements of MMC-HA resulted in a corrosion rate of 1.25 ± 0.16 mm/year which was lower than the corrosion rates (2.0-3.2 mm/yr) determined in the immersion test, while volume changes in SRμCT during the first 20 hours were too low for reliable calculation of the corrosion rate. The scatter in electrochemical measurements of MMC-HA was interpreted as a break down and reformation of the protective surface layer. The break down of the protective layer was responsible for the observed localised corrosion and occurred randomly during the whole test period. However, compared to the AZ91D matrix sample, it is most likely that especially the localised corrosion attacks, which were responsible for the major weight loss in the immersion tests, required some initiation time in MMC-HA samples. In contrast, the MMC-HA showed a more uniform corrosion in cell solution which might be due to the lower chloride concentration in the cell solution. The addition of proteins to the cell solution increased the corrosion rate of the MMC-HA slightly, but did not change the corrosion morphology. This finding is based most likely on the changed corrosive media which can influence surface roughness, electrostatic forces as well as protein adhesion to metals and therefore result in different corrosion behaviour [23;24]. In this study the corrosion behaviour of the MMC-HA was strongly determined by the formation of passive layers on the specimen surfaces, as shown for MMCs in different corrosive environments [25]. While pitting occurred in artificial sea water, a white un-uniform layer

was found on the MMC-HA samples consisting of amorphous $CaCO_3$. However, after immersion of MMC-HA samples in cell solutions with and without proteins an uniform black layer was observed which protected successfully the sample surfaces. However, X-ray diffraction showed no formation of $CaCO_3$. SRμCT revealed that the deposition of $CaCO_3$ occurred mainly during the first 9-14 hours after immersion in artificial sea water on MMC-HA as well as on AZ91D samples, where shallow pits as well as uncorroded surfaces were covered by $CaCO_3$. These precipitations seemed to reduce the local corrosion attack and led to more uniform corrosion with MMC-HA, while uncovered areas of AZ91D exhibited severe pitting and high corrosion rates. Magnesium ions which are present at high concentrations on the corroding surface are known as a crystallisation inhibitor and especially as a stabiliser of amorphous calcium carbonates [26]. The microporosity of precipitated calcium carbonates may explain that magnesium corrosion is reduced but not inhibited [27]. The excellent cytocompatiblity, the low solubility of calcium carbonates as well as the additional stabilization of $CaCO_3$ by organic additives [26-28] favours them as a protective coating on future magnesium implants.

The cytocompatibility tests using MTT assay [10] have been used to determine the cytotoxicity of cobalt and chromium metal ions [29] and composite materials including hydroxyapatite [30]. In this study it was shown that macrophages, osteoblasts and human derived bone cells adhere, proliferate and survive on the corroding surface of MMC-HA in a cell culture system comparable to the cell viability on tissue culture plastic, or even better. These findings are in accordance with the previously reported cytoprotective effects of magnesium on bovine endothelial cells [31] and the positive effect of elevated magnesium concentration on proliferation and cell viability of neural cells [32].

5. Conclusion

In summary, our results clearly show that magnesium alloy-based metal matrix composites are novel cytocompatible metals with adjustable mechanical and corrosive properties. The distribution and size of the hydroxyapatite particles are of major importance for mechanical and corrosive properties. In contrast to previous studies, the addition of hydroxyapatite particles enhanced the corrosion resistance of the magnesium matrix in artificial sea water and cell solutions. Further studies will focus on combinations of different magnesium alloys as MMC matrix and on the selection of biocompatible particles.

Acknowledgements

We thank E. Hille and S. Dries, Hospital Eilbek, Hamburg for the bone samples, J. Schnieders, University of Marburg for the donation of MG-63 cells. RAW264.7-cells were a kind gift of A. Gasser, University Hospital Eppendorf, Hamburg. K. Pfaffenbach, GKSS Research Centre, is acknowledged for the sample sterilisation.

References

[1] Clyne TW. Vol.3 of Comprehensive Composite Materials. Pergamon, 2000.

[2] Foltz JV, Blackmon CM. Metal matrix composites. Advanced Materials and Processes 1998;154:19-23.

[3] Landkof B. Development of high strength magnesium based MMC reinforced with SiC particles for satellite structure applications. Materialwissenschaft und Werkstofftechnik 2003;34:395-399.

[4] Beck A. Magnesium und seine Legierungen. Berlin: Springer-Verlag; 1939.

[5] Emley EF. Principles of magnesium technology. Oxford: Pergamon Press; 1966.

[6] Fulmer MT, Ison IC, Hankermayer CR, Constantz BR, Ross J. Measurements of the solubilities and dissolution rates of several hydroxyapatites. Biomaterials 2002; 23:751-755.

[7] Tadic D, Epple M. A thorough physicochemical characterisation of 14 calcium phosphate-based bone substitution materials in comparison to natural bone. Biomaterials 2004;25:987-994.

[8] Witte F, Kaese V, Haferkamp H, Switzer E, Meyer-Lindenberg A, Wirth CJ et al. In vivo corrosion of four magnesium alloys and the associated bone response. Biomaterials 2005;26:3557-3563.

[9] Witte F, Fischer J, Nellesen J, Crostack HA, Kaese V, Pisch A et al. In vitro and in vivo corrosion measurements of magnesium alloys. Biomaterials 2006;27:1013-1018.

[10] Ciapetti G, Cenni E, Pratelli L, Pizzoferrato A. In vitro evaluation of cell/biomaterial interaction by MTT assay. Biomaterials 1993;14:359-364.

[11] Kree V, Bohlen J, Letzig D, Kainer KU. The metallographical examination of magnesium alloys. Practical Metallography 2004;41:233-246.

[12] PDF. The Powder Diffraction FileTM. International Center for Diffraction Data (ICDD), PDF Release 2002, web site: www icdd com 2002.

[13] Gallagher JA, Beresford JN, McGuire MK, Ebsworth NM, Meats JE, Gowen M et al. Effects of glucocorticoids and anabolic steroids on cells derived from human skeletal and articular tissues in vitro. Adv Exp Med Biol 1984; 171:279-291.

[14] Sudarsanan K, Young RA. Strontium apatite structures. Journal of Dental Research 1973;52:112.

[15] Currey J, Brear K. Hardness, Young's modulus and yield stress in mammalian mineralized tissues. J.Mater.Sci.Mater.Med. 1990;1:14-20.

[16] Evans P, Behiri J, Currey J, Bonfield W. Microhardness and Young's modulus in cortical bone exhibiting a wide range of mineral volume fractions and in a bone analogue. J.Mater.Sci.Mater.Med. 1990;1:38-43.

[17] Caceres C, Poole W, Bowles A, Davidson C. Section thickness, marcohardness and yield strength in hpdc magnesium alloy AZ91. Materials SCience and Enginering A 2005;402:269-277.

[18] Tabor D. The Hardness of Metals. London: Oxford University Press; 1951.

[19] Hodgskinson R, Currey JD, Evans GP. Hardness, an indicator of the mechanical competence of cancellous bone. J Orthop Res 1989;7:754-758.

[20] Staiger MP, Pietak AM, Huadmai J, Dias G. Magnesium and its alloys as orthopedic biomaterials: a review. Biomaterials 2006;27:1728-1734.

[21] Nunez-Lopez CA, Skeldon P, Thompson GE, Lyon P, Karimzadeh H, Wilks TE. The corrosion behaviour of Mg alloy ZC71/SiC"SUB p" metal matrix composite. Corrosion Science 1995;37:689-708.

[22] Chan WM, Cheng FT, Leung LK, Horylev RJ, Yue TM. Corrosion behaviour of magnesium alloy AZ91 and ITS MMC in NaCl solution. Corrosion Reviews 1998; 16:43-52.

[23] Williams RL, Brown SA, Merritt K. Electrochemical studies on the influence of proteins on the corrosion of implant alloys. Biomaterials 1988;9:181-186.

[24] Williams RL, Williams DF. Albumin adsorption on metal surfaces. Biomaterials 1988;9:206-212.

[25] Zucchi F, Trabanelli G, Grassi V, Frignani A. Corrosion behavior in sodium sulfate and sodium chloride solutions of SiCp reinforced magnesium alloy metal matrix composites. Corrosion 2004;60:362-368.

[26] Loste E, Wilson RM, Seshadri R, Meldrum FC. The role of magnesium in stabilising amorphous calcium carbonate and controlling calcite morphologies. Journal of Crystal Growth 2003;254:206-218.

[27] Combes C, Miao B, Bareille R, Rey C. Preparation, physical-chemical characterisation and cytocompatibility of calcium carbonate cements. Biomaterials 2006; 27:1945-1954.

[28] Brecevic L, Nielsen AE. Solubility of amorphous calcium carbonate. Journal of Crystal Growth 1989;98:504-510.

[29] Fleury C, Petit A, Mwale F, Antoniou J, Zukor DJ, Tabrizian M et al. Effect of cobalt and chromium ions on human MG-63 osteoblasts in vitro: Morphology, cytotoxicity, and oxidative stress. Biomaterials 2006;27:3351-3360.

[30] Marques AP, Reis RL, Hunt JA. The biocompatibility of novel starch-based polymers and composites: In vitro studies. Biomaterials 2002;23:1471-1478.

[31] Mak IT, Komarov AM, Kramer JH, Weglicki WB. Protective mechanisms of Mg-gluconate against oxidative endothelial cytotoxicity. Cellular and Molecular Biology 2000;46:1337-1344.

[32] Krueger RC, Santore MT, Dawson G, Schwartz NB. Increased extracellular magnesium modulates proliferation in fetal neural cells in culture. Developmental Brain Research 2001;127:99-109.

Figure Captions

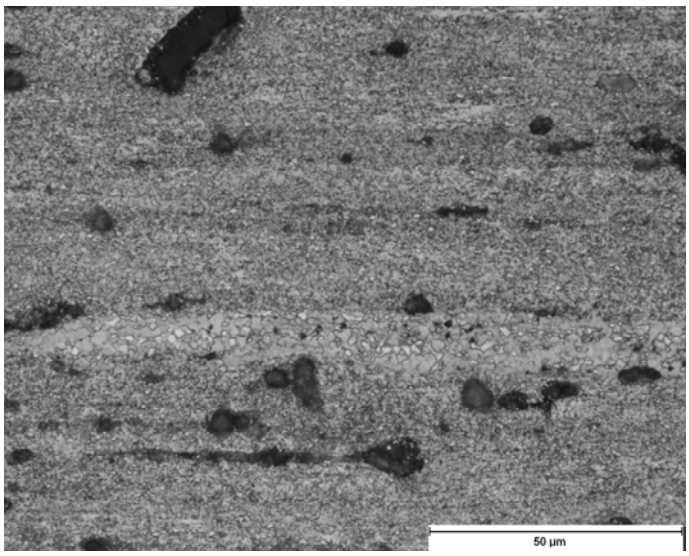

Figure 1: Microstructure of the longitudinal direction of MMC-HA. The extrusion direction is orientated horizontally. Black inclusions represent agglomerated HA particles in the AZ91D matrix.

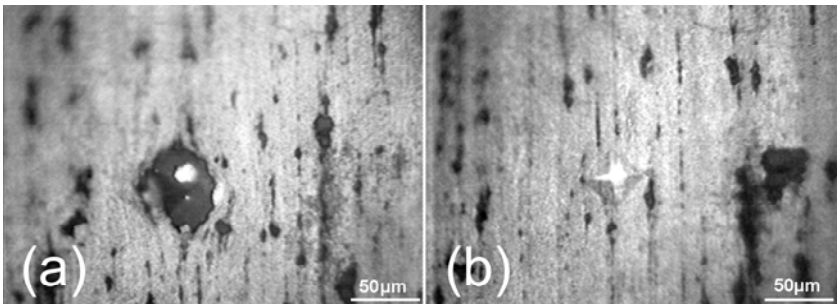

Figure 2: Microstructure of MMC-HA showing HA conglomerates in the matrix with Vickers hardness indents in different areas of the MMC-HA sample. Large HA conglomerates cause low Vickers hardness (a: $HV_{0.1} = 63$), while homogenous distribution of small HA particles result in high Vickers hardness (b: $HV_{0.1} = 98$).

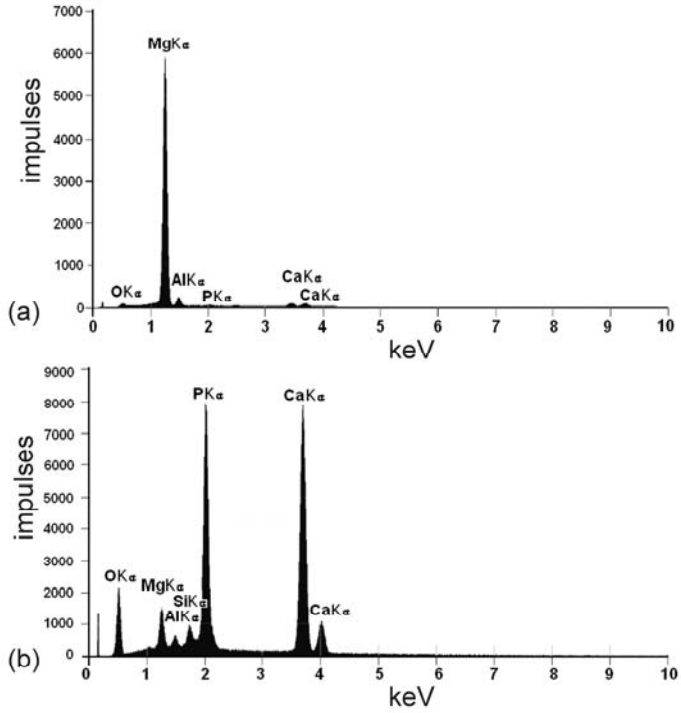

Figure 3: EDX analysis (a) of the matrix composition and (b) the HA formation in the MMC-HA sample.

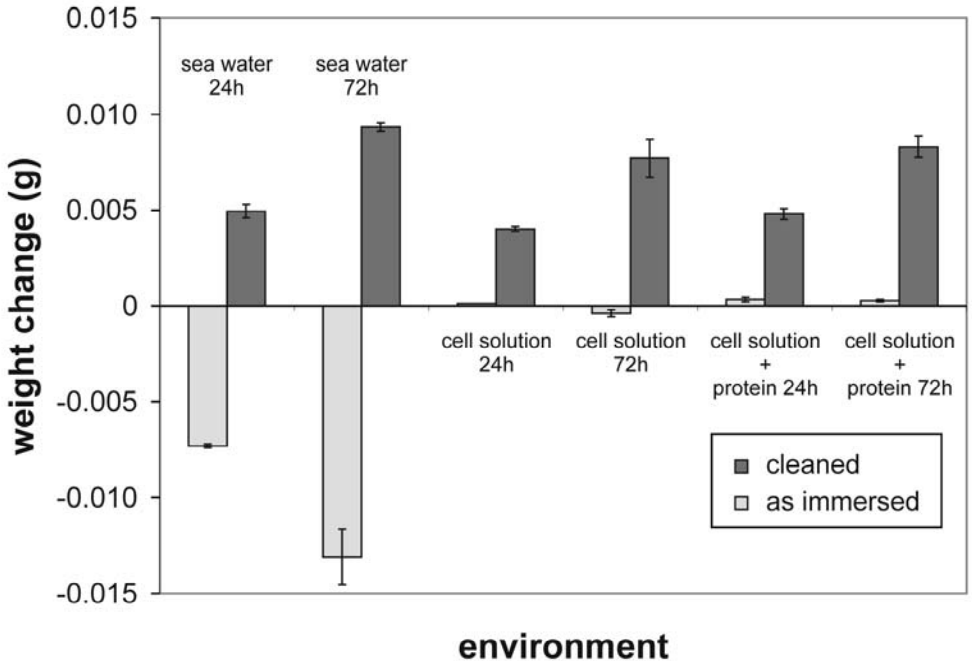

Figure 4: Weight changes of immersed MMC-HA samples in artificial sea water, cell solutions with and without proteins after 24 and 72 hours (negative values indicate weight

gains, while positive values indicate weight losses). The weights after the immersion test were determined with and without (as immersed) cleaning of the surface in chromic acid.

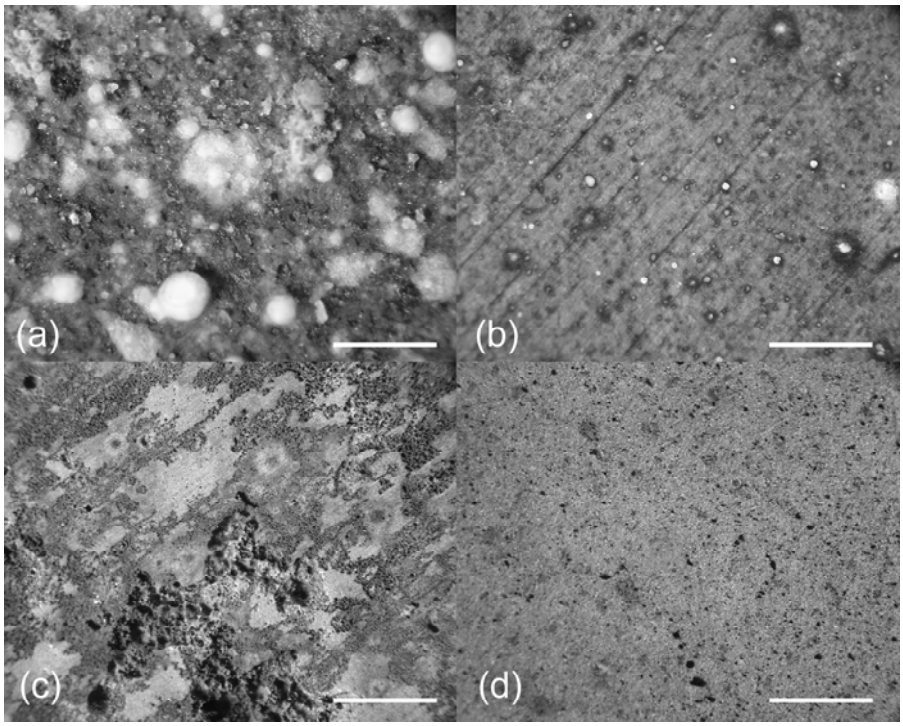

Figure 5: Surface appearance after 72 hours of immersion in a) artificial sea water, b) cell solution with protein, c) artificial sea water (cleaned) and d) cell solution with protein (cleaned).

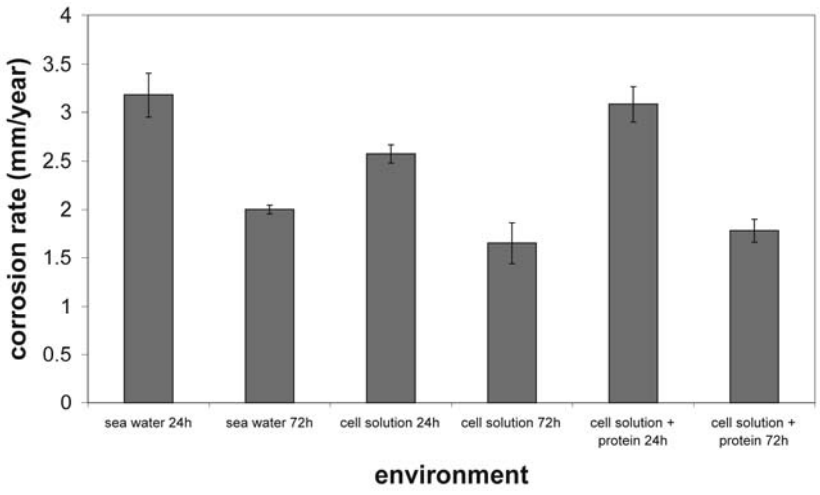

Figure 6: Calculated corrosions rates after 24 and 72 hours of immersion in various corrosive environments.

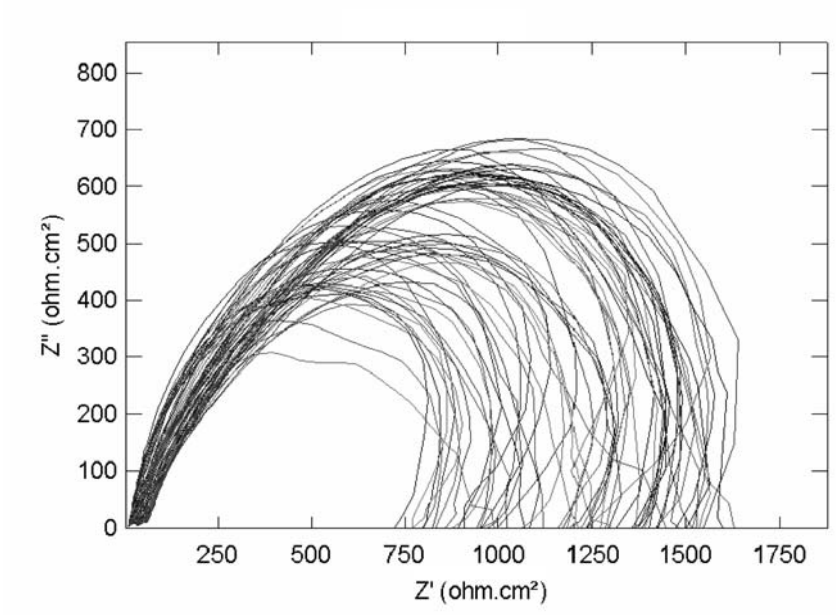

Figure 7: Typical EIS spectra recorded over a period of 72 hours with a measurement every hour for a specimen immersed in artificial sea water at 37°C.

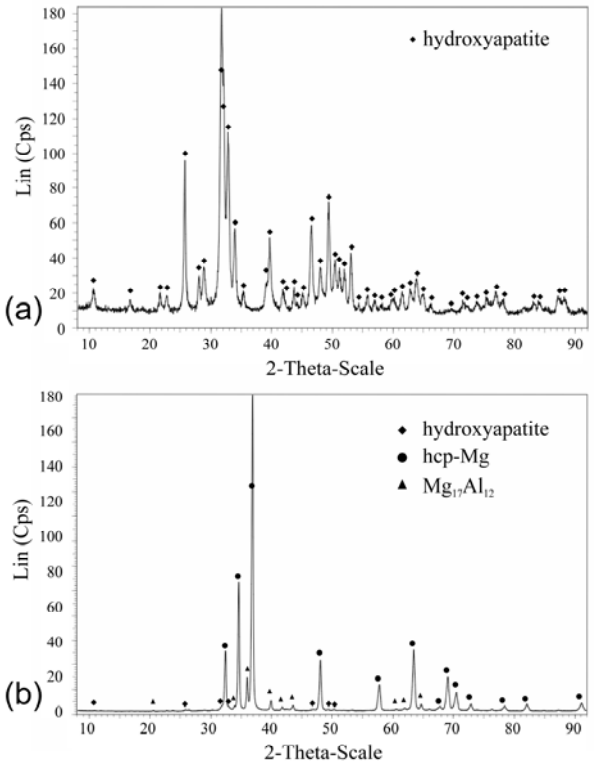

Figure 8: The diffraction pattern (a) showing reflections of hydroxyapatite $Ca_{10}(PO_4)_6(OH)_2$, while (b) shows the diffraction pattern of the extruded MMC-HA sample.

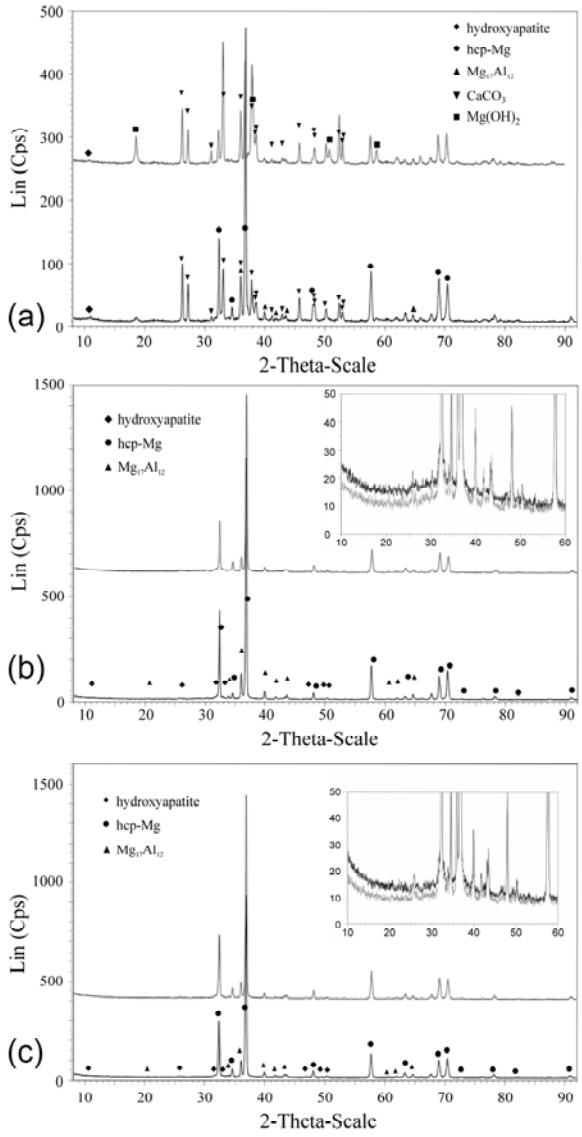

Figure 9: Diffraction pattern of the MMC-HA samples (a) after immersion in artificial sea water for 24 (lower line) and 72 hours (upper line), after immersion in cell solution for 24 (lower line) and 72 hours (upper line) without (b) and with proteins (c). Insert shows peak broadening indicating amorphous phases on the MMC-HA samples.

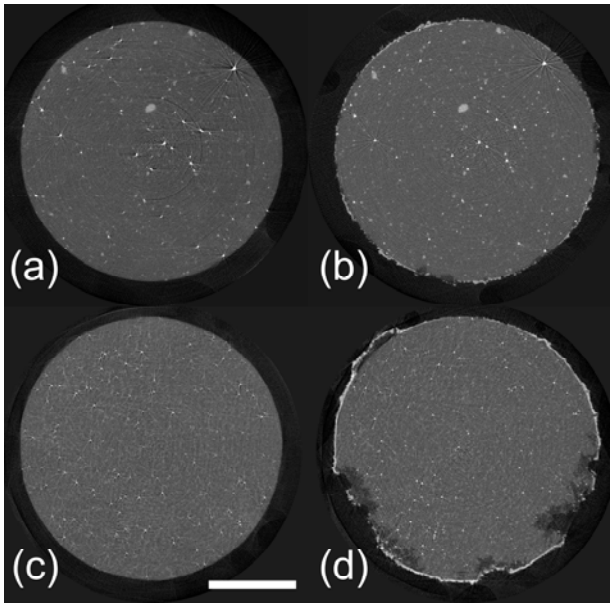

Figure 10: Two-dimensional reconstruction of MMC-HA sample (a, b) and AZ91D sample (c, d) immersed in artificial sea water at 37°C at time point 0 (a,c) and after 20 hours (b,d). Severe localized corrosion attack can be observed on the AZ91D sample after 20 hours of immersion (d), while the MMC-HA exhibited minor corrosion attack (b). Scale bar = 1 mm.

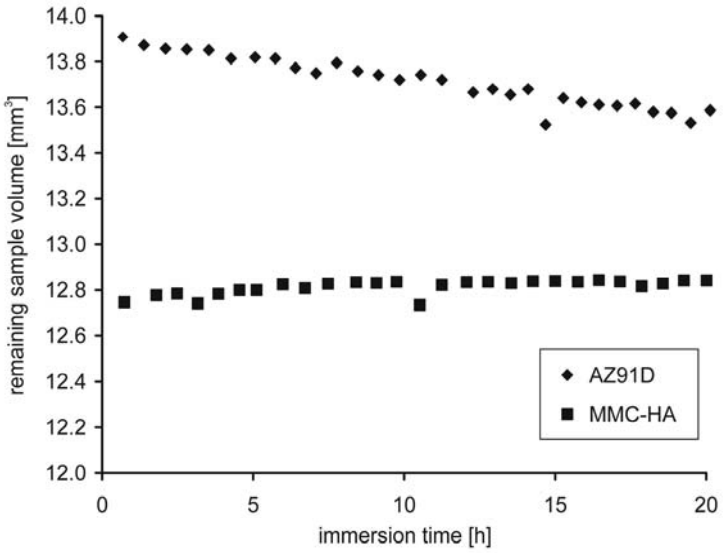

Figure 11: The diagram shows the remaining metal volume of immersed magnesium samples over 20 hours of immersion in artificial sea water at 37°C. The MMC-HA sample (square) did not change significantly in volume, while the AZ91D volume was decreased by pitting corrosion (rhombus).

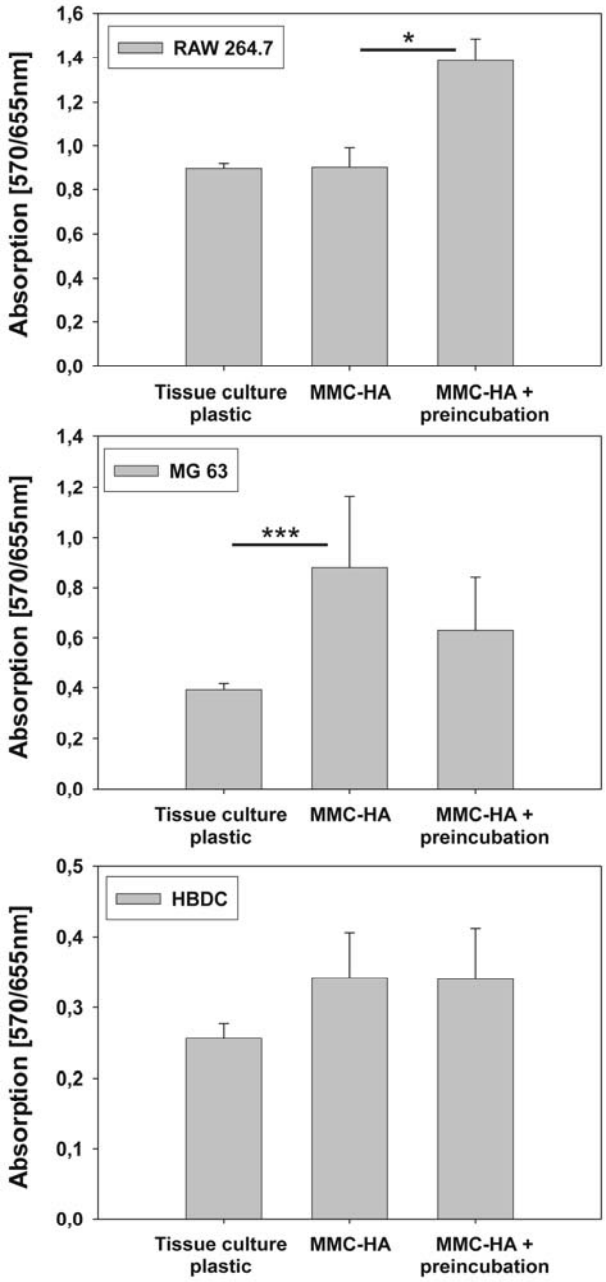

Figure 12: MTT-assay of Raw 264.7 macrophages, MG-63 human osteosarcoma cells and human bone derived cells (HBDC) cultured on MMC-HA with and without preincubation in protein solution. Cells cultured on tissue culture plastic served as a control. The initial cell seeding density was $5 \cdot 10^4$ (RAW264.7, MG-63), or $2 \cdot 10^4$ cells/carrier (HBDC). Statistical significance between groups are indicated by asterisks (* = $p < 0.05$; *** = $p < 0.001$).

Tables

Table 1: Representative composition in weight percent (wt. %) of matrix and HA conglomerates.

Position	**Composition in wt. %**					
	Al	Zn	Si	Ca	P	Mg
MMC Matrix	8.31	1.09				balance
HA conglomerates	1.14		1.77	61.21	31.12	4.75

Table 2: pH of cell culture medium measured 2 days after incubation with MMC-HA or tissue culture plastic or without any sample inside a tissue culture well.

Samples	**Mean value**	**Standard deviation**	**N**
Fresh medium, no sample	7.17	± 0.01	10
Medium + Tissue culture plastic	7.91	± 0.07	10
Medium + MMC-HA	8.12	± 0.07	10